Journal of the Optical Society of America B
OPTICAL PHYSICS

Second-harmonic generation from plasmon polariton excitation on silver diffraction gratings: comparisons of theory and experiment

Marina E. Inchaussandague,[1,2,*] Miriam L. Gigli,[3] Kevin A. O'Donnell,[4] Eugenio R. Méndez,[4] Renato Torre,[5] and Claudio I. Valencia[6]

[1]Universidad de Buenos Aires, Facultad de Ciencias Exactas y Naturales, Departamento de Física, Grupo de Electromagnetismo Aplicado, Buenos Aires, Argentina
[2]Consejo Nacional de Investigaciones Científicas y Técnicas, Instituto de Física de Buenos Aires (IFIBA), Buenos Aires, Argentina
[3]Universidad de Buenos Aires, Ciclo Básico Común, Departamento de Ciencias Exactas, Buenos Aires, Argentina
[4]División de Física Aplicada, Centro de Investigación Científica y de Educación Superior de Ensenada, Carretera Ensenada-Tijuana No. 3918, Ensenada, B.C. 22860, Mexico
[5]European Laboratory for Non-Linear Spectroscopy (LENS), Universitá di Firenze, Via N. Carrara 1, I-50019 Sesto Fiorentino, Firenze, Italy
[6]Facultad de Ciencias, Universidad Autónoma de Baja California, Km. 103 Carretera Ensenada-Tijuana, Ensenada, B.C. 22860, Mexico
*Corresponding author: mei@df.uba.ar

Received 14 September 2016; revised 2 November 2016; accepted 4 November 2016; posted 7 November 2016 (Doc. ID 275781); published 2 December 2016

We present a comparison between experimental and theoretical results for the diffraction efficiencies of the second-harmonic light produced in the orders of silver diffraction gratings. The gratings considered are sinusoidal, have depths of a few nanometers, and can produce significant surface plasmon polariton excitation at fundamental and second-harmonic frequencies. The calculations are based on a general expression for the nonlinear polarization of the surface of a homogeneous and isotropic medium, and the diffraction problems at the fundamental and harmonic frequencies are solved using a Rayleigh method. The silver gratings were fabricated using holographic lithography and evaporative metal deposition techniques. The samples were illuminated with picosecond pulses of wavelength 1064 nm, and photon-counting techniques were used to study the diffracted orders at 532 nm, with absolute normalization provided by a quartz reference. The diffracted orders exhibit anomalies and other features, many of which are related to plasmon polariton excitation at both fundamental and second-harmonic frequencies. Employing previously measured values for the nonlinear susceptibilities of a flat silver surface, remarkably good comparisons of theory and experiment are obtained for the second-harmonic order efficiencies.

OCIS codes: (240.4350) Nonlinear optics at surfaces; (240.6680) Surface plasmons; (050.2770) Gratings.

https://doi.org/10.1364/JOSAB.34.000027

1. INTRODUCTION

The resonant interaction of light with free surface charges produces optical effects that have been known and used in applications for quite some time. One of the first and better-known theoretical studies on the subject is that of Maxwell Garnett [1], who provided an explanation for the colors of metal films and colloids. The field, known now as plasmonics [2–6], has experienced several periods of revival over the years and constitutes now one of the most active fields of research in optics. This renewed interest in the field is partly due to the possibilities offered by the use of these collective excitations for enhancing surface fields and for confining light into spaces with subwavelength dimensions. The field enhancements associated with the excitation of either surface plasmon polaritons (SPPs) or localized surface polaritons facilitates the observation of weak nonlinear effects that depend strongly on local surface fields. Plasmonics also provides some of the building blocks for the design of optical metamaterials.

Second-harmonic generation (SHG) from flat metallic surfaces has been studied since the 1960s [7–11]. The signals are weak and sensitive to the state of the surface because, for materials with inversion symmetry, the electric dipole contribution to the second-order nonlinear susceptibility vanishes. Since those times, efforts have been made to better understand the observed effects and to model the relevant nonlinearities [12–22]. The simple models that have been developed for this purpose are helpful for the visualization of the physical mechanisms responsible for SHG, but they are insufficient to accurately estimate the

material-dependent nonlinear surface susceptibilities. In this respect, the recent measurements of the SHG from a flat evaporated silver surface for various combinations of the incident and second-harmonic polarization, which permits the determination of the three independent elements of the nonlinear surface susceptibility tensor, constitute an encouraging new development [23].

Due to the excitation of SPPs, the second-harmonic (SH) signals obtained from structured surfaces can be significantly higher than those obtained from flat ones. Metallic diffraction gratings [24–30], as well as periodic arrays of nanoparticles [31] and nanoapertures [32,33] that support plasmonic resonances, have been the subject of several studies (see the recent reviews in Refs. [34,35]). Similarly, the introduction of random roughness can increase the SH signals through both multiple scattering effects and the excitation of SPPs [36–42]. A noteworthy feature in the angular distribution of the SH light scattered by randomly rough surfaces is the presence of a dip in the backscattering direction, which is due to the destructive interference between multiply scattered waves [38–42].

Also motivated by the possibility of enhancing the SH efficiency, there have been studies of the nonlinear efficiency of samples containing periodic arrays of nonsymmetrical particles [43]. It has been found that with samples containing periodic arrays of L-shaped nanoparticles, the SH efficiency depends strongly on the polarization of the incident field [44] and that the second-order susceptibility tensor contains components that are forbidden in symmetric systems [45]. More recently, SHG from particles that support magnetic resonances, like split-ring resonators (SRRs), have also attracted some attention. The first studies of SHG with resonant SRRs suggested that the excitation of magnetic resonances was favorable for the effect [46,47]. However, later studies employing complementary SRRs, in which the roles of the electrical and magnetic resonances are interchanged, did not confirm that suggestion [48].

It can be said that, in general, as more stable and powerful laser sources have become available at a variety of wavelengths, the quality and accuracy of the experimental results have improved over time. There have also been significant advances in the fabrication and characterization of samples at the nanoscale, and numerical work has benefited from the availability of more powerful computers and by the development of sophisticated computational techniques for electromagnetic calculations. Nevertheless, a common feature in all the work reported with nonplanar surfaces and particles is the lack of detailed and quantitative comparisons between theory and experiment. This situation attests, on one hand, to the experimental difficulties associated with the characterization of the sample and the normalization of the data (usually, SH intensity data are presented in arbitrary units) and, on the other hand, to the lack of simple models for quantitative calculations of the nonlinear response of the surface.

In this paper, we present direct comparisons of theoretical and experimental results for the efficiencies of the second-harmonic diffracted orders produced by well-characterized silver gratings. The gratings have shallow sinusoidal profiles and the effects of surface plasmon polariton excitation are strong, both at the fundamental and second-harmonic frequencies. The calculations are carried out using the experimentally determined nonlinear susceptibilities for flat silver surfaces reported in Ref. [23]. The agreement between the experimental and theoretical results demonstrates that these flat-surface susceptibilities can be used for calculations involving nonplanar surfaces and the excitation of SPPs. The presentation of quantitative comparisons between theory and experiment, together with the significance of this conclusion, represent the distinguishing features of this work. Further, the theory is here compared with data that are properly normalized and extend over a dynamic range of approximately five orders of magnitude, which is quite novel in such work.

The paper is organized as follows. In Section 2, we present our theoretical formulation, which is based on a completely general expression for the nonlinear polarization of a homogeneous and isotropic medium. The generated second-harmonic field contains contributions from the bulk of the metal, due to the gradients of the fundamental field in the medium, and from the surface, due to the abrupt change in the material properties at the interface. The diffracted linear and nonlinear fields are calculated with a Rayleigh method [49,50]. In Section 3, we describe the experimental work, carried out with two sinusoidal silver diffraction gratings fabricated by holographic methods. The gratings were illuminated with 100 ps pulses of 1064 nm wavelength light, and the diffracted orders at the second-harmonic wavelength of 532 nm were detected with photon-counting techniques; the normalization was provided by comparison with the second-harmonic signals obtained from a quartz reference sample. Theoretical and experimental results are presented together in Section 4. The theoretical results were obtained with the values of the three nonlinear flat-surface susceptibilities determined experimentally in Ref. [23]. Finally, conclusions drawn from the observed features and the direct comparisons between theoretical and experimental results are presented in Section 5.

2. THEORY

When an electromagnetic field impinges upon a periodic surface, the reflected field at the original frequency ω consists of a series of diffraction orders. Of particular relevance to the work presented here is the fact that, due to the nonlinearities of the material, the diffracted field may also contain diffraction orders at 2ω. In this section, we describe the theoretical approach employed to solve this nonlinear diffraction problem. When possible, we shall omit details that can be found in previous publications on the subject [51,52] that dealt only with the case of p-polarized illumination.

The diffracted fields at the fundamental and harmonic frequencies are found by writing the propagation equations in each medium and imposing the boundary conditions at the interface between them. Since the second-harmonic radiation is generated at the surface, the sources of the second-harmonic field may be represented by discontinuities in the tangential components of the fields at the interface between the two media. The strength of these discontinuities depends on the constants that define the nonlinear properties of the nonlinear medium and on the solution of the problem at the fundamental frequency.

A. Nonlinear Sources

We consider a periodically corrugated boundary separating a linear medium (I) and a nonlinear material (II). Both media

are assumed isotropic, homogeneous, and nonmagnetic. The permittivities of the media are denoted by $\varepsilon_{\mathrm{I}}(\Omega)$ for medium I and $\varepsilon_{\mathrm{II}}(\Omega)$ for medium II, where Ω stands for the fundamental (ω) or second-harmonic (2ω) frequencies. As shown in Fig. 1, we consider a coordinate system (x_1, x_2, x_3), in which the grooves of the grating are along the x_2 axis and the x_3 axis is perpendicular to the mean surface of the grating, pointing toward the linear medium. A local system of coordinates (x, y, z) aligned with the normal to the surface at each point is also employed in the theory. The grating profile is described through the vector-valued function $\mathbf{r}_s(t) = f(t)\hat{x}_1 + g(t)\hat{x}_3$, where the functions $f(t)$ and $g(t)$ are single-valued functions of the parameter t, $\phi(t) = \{[f'(t)]^2 + [g'(t)]^2\}^{1/2}$ is a function that will appear in the diffraction calculations, and the primes denote derivatives with respect to t.

To calculate the field at the second-harmonic frequency, we assume a nonlinear polarization of the form [10]

$$\mathbf{P}^{\mathrm{NL}}(\mathbf{r}|2\omega) = \alpha[\mathbf{E}(\mathbf{r}|\omega)\cdot\nabla]\mathbf{E}(\mathbf{r}|\omega) + \beta\mathbf{E}(\mathbf{r}|\omega)[\nabla\cdot\mathbf{E}(\mathbf{r}|\omega)] + \gamma\nabla[\mathbf{E}(\mathbf{r}|\omega)\cdot\mathbf{E}(\mathbf{r}|\omega)], \tag{1}$$

where $\mathbf{E}(\mathbf{r}|\omega)$ represents the electric field at the fundamental frequency, and α, β, and γ are frequency-dependent parameters that characterize the bulk nonlinear response of the medium.

We assume that the grating is illuminated by a purely *s*- or *p*-polarized plane wave of frequency ω, whose time dependence of the type $\exp(-i\omega t)$ is considered but suppressed from the notation. A property of the problem that we exploit in the calculations is that, due to the invariance of the system along x_2, the *s* and *p* fields at the frequency ω are uncoupled and can be treated separately. Also, in what follows, we shall denote the components of the electric (*s* polarization) or magnetic (*p* polarization) fields along x_2 by $\psi^{(\mathcal{R})}_{s,p}(\mathbf{r}|\Omega)$, where $\mathcal{R}$ represents region I or II, and Ω stands for ω or 2ω.

It is known that for the excitation conditions considered (incident field purely *s*- or *p*-polarized), the fields satisfy homogeneous Helmholtz equations at the two frequencies and there is no *s*-polarized second-harmonic radiation {see Eqs. (18), (19b), (22a), and (22b) of Ref. [51]}. Therefore, the second-harmonic diffracted field is generated by surface sources and is always *p*-polarized.

The nonlinear boundary conditions satisfied by the (*p*-polarized) harmonic field can be written in the general form [51]

$$\psi_p^{(\mathrm{I})}(t|2\omega) - \psi_p^{(\mathrm{II})}(t|2\omega) = A_p(t|\omega), \tag{2a}$$

$$\frac{1}{\varepsilon_{\mathrm{I}}(2\omega)}\Upsilon_p^{(\mathrm{I})}(t|2\omega) - \frac{1}{\varepsilon_{\mathrm{II}}(2\omega)}\Upsilon_p^{(\mathrm{II})}(t|2\omega) = B_p(t|\omega), \tag{2b}$$

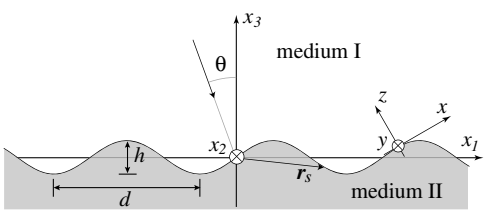

Fig. 1. Illustration of the grating profile and the coordinate systems considered.

where $\psi_p^{(\mathrm{I,II})}(t|2\omega)$ and $\Upsilon_p^{(\mathrm{I,II})}(t|2\omega)$ are the x_2 components of, respectively, the magnetic field and its normal derivative, both evaluated at the surface. The nonlinear sources $A_p(t|\omega)$ and $B_p(t|\omega)$ that appear on the right-hand side of Eq. (2) are responsible for the generation of the second-harmonic field and can be determined from the solutions of the electromagnetic problem at frequency ω and the nonlinear properties of the material.

Starting from the expressions found in Ref. [51], and after some algebra, one can find the following expressions for these nonlinear sources:

$$A_p(t|\omega) = 8\pi i\frac{c}{\omega}\frac{\chi_{\parallel\parallel\perp}}{\varepsilon_{\mathrm{I}}(\omega)}\frac{1}{\phi^2(t)}\Upsilon_p^{(\mathrm{I})}(t|\omega)\frac{d\psi_p^{(\mathrm{I})}(t|\omega)}{dt}, \tag{3a}$$

$$B_p(t|\omega) = 8\pi i\frac{c}{\omega}\left[\chi_{\perp\perp\perp}\frac{d}{dt}\left(\frac{1}{\phi(t)}\frac{d\psi_p^{(\mathrm{I})}(t|\omega)}{dt}\right)^2 + \frac{\chi_{\perp\parallel\parallel}}{\varepsilon_{\mathrm{I}}^2(\omega)}\frac{d}{dt}\left(\frac{\Upsilon_p^{(\mathrm{I})}(t|\omega)}{\phi(t)}\right)^2 + \chi_b\frac{d[\psi_p^{(\mathrm{I})}(t|\omega)]^2}{dt}\right] - 8\pi i\frac{\omega}{c}\eta_{\perp\parallel\parallel}\frac{d[\psi_s^{(\mathrm{I})}(t|\omega)]^2}{dt}, \tag{3b}$$

where, as usual, c represents the speed of light in vacuum. The second-order susceptibilities that appear in these equations are related to the bulk nonlinear constants that appear in Eq. (1) and to the elements of the second-order surface susceptibility tensor χ^s_{ijk} defined in Refs. [51,52], as follows:

$$\chi_{\parallel\parallel\perp} = \chi^s_{ttz}, \tag{4a}$$

$$\chi_{\perp\perp\perp} = \chi^s_{zzz} + \frac{\alpha/2+\gamma}{\varepsilon_{\mathrm{II}}(2\omega)\varepsilon_{\mathrm{II}}^2(\omega)}, \tag{4b}$$

$$\chi_{\perp\parallel\parallel} = \chi^s_{ztt} + \frac{\alpha/2+\gamma}{\varepsilon_{\mathrm{II}}(2\omega)}, \tag{4c}$$

$$\eta_{\perp\parallel\parallel} = \chi^s_{ztt} + \frac{\gamma}{\varepsilon_{\mathrm{II}}(2\omega)}, \tag{4d}$$

$$\chi_b = \frac{\alpha}{2\varepsilon_{\mathrm{II}}(\omega)\varepsilon_{\mathrm{II}}(2\omega)}\left(\frac{\omega}{c}\right)^2, \tag{4e}$$

where terms containing α and/or γ are bulk contributions. These expressions demonstrate that, to solve the second-harmonic diffraction problem, it is not necessary to know the bulk and surface susceptibilities individually but only certain combinations of them.

B. Rayleigh Expansions

In the present paper, the electromagnetic fields at ω and 2ω are calculated using a standard Rayleigh method [53–56]. In particular, it is assumed that the fields can be represented by Rayleigh expansions in the region between the grooves (Rayleigh hypothesis).

Therefore, we write the second-harmonic fields in media I and II as

$$\psi_p^{(\mathrm{I})}(\mathbf{r}|2\omega) = \sum_{n=-\infty}^{\infty} U_n \exp[i(\alpha_n^{2\omega} x_1 + \beta_n^{2\omega} x_3)], \tag{5a}$$

$$\psi_p^{(\mathrm{II})}(\mathbf{r}|2\omega) = \sum_{n=-\infty}^{\infty} V_n \exp[i(\alpha_n^{2\omega} x_1 + \gamma_n^{2\omega} x_3)], \tag{5b}$$

where

$$(\alpha_n^{2\omega})^2 + (\beta_n^{2\omega})^2 = \varepsilon_{\mathrm{I}}(2\omega)\left(\frac{2\omega}{c}\right)^2, \tag{6a}$$

$$(\alpha_n^{2\omega})^2 + (\gamma_n^{2\omega})^2 = \varepsilon_{\mathrm{II}}(2\omega)\left(\frac{2\omega}{c}\right)^2, \tag{6b}$$

$$\alpha_n^{2\omega} = \frac{2\omega}{c}\sin\theta + n\frac{2\pi}{d}, \tag{6c}$$

θ is the angle of incidence, d is the period of the grating, and n is an integer. To solve the electromagnetic problem at 2ω, we truncate Eqs. (5a) and (5b) from $-M$ to M and then substitute these equations into the left-hand side of Eqs. (2a) and (2b), thus obtaining a system of $2(2M+1)$ equations that can be used to determine the $2(2M+1)$ unknown amplitudes U_n and V_n (see Ref. [52]). In matrix form, the system of equations can be written as

$$\begin{bmatrix} u_m^{\kappa} \\ v_m^{\kappa} \end{bmatrix} = \begin{bmatrix} A_{nm}^{>} & A_{nm}^{<} \\ B_{nm}^{>} & B_{nm}^{<} \end{bmatrix} \begin{bmatrix} U_n \\ V_n \end{bmatrix}, \tag{7}$$

where κ stands for s or p polarization. Equation (7) is a generalization of Eq. (30) of Ref. [52] that includes the case of incidence with s-polarized light. Expressions for the nonlinear source coefficients u_m^{κ} and v_m^{κ} as well as of the matrix elements $A_{nm}^{>}$, $A_{nm}^{<}$, $B_{nm}^{>}$, and $B_{nm}^{<}$ are given in Appendix A. Once the unknown amplitudes U_n and V_n are calculated, the power of each diffracted order follows directly.

C. Efficiency of the Second-Harmonic Radiation

To determine the second-harmonic diffraction efficiency, we start by considering a uniform beam of power P_i and transverse area A_i that is incident on the grating. The power $P_n^{2\omega}$ of the nth reflected order at 2ω is proportional to the square of P_i and inversely proportional to A_i so that $P_n^{2\omega} \propto P_i^2/A_i$. It is convenient to normalize the reflected power at 2ω in such a way that the results are independent of P_i and A_i. We thus define the efficiency of the nth second-harmonic diffracted order as

$$R_n(2\omega) = \frac{P_n^{2\omega} A_i}{(P_i)^2}. \tag{8}$$

This quantity can also be expressed in terms of the moduli of the time-averaged Poynting vectors of the incident and nth-order diffraction fields as follows:

$$R_n(2\omega) = \frac{S_n^{2\omega}\cos\theta_n}{(S_i)^2\cos\theta}. \tag{9}$$

The time-averaged Poynting vector associated with the nth second-harmonic order is given by the expression

$$\langle \mathbf{S}_n^{2\omega} \rangle = \frac{c^2}{16\pi\omega}\Re e[i\mathbf{H}_n \times (\nabla \times \mathbf{H}_n)^*], \tag{10}$$

where $\Re e[\cdot]$ denotes the real part, the angle brackets denote a time average, and

$$\mathbf{H}_n(x_1, x_3|2\omega) = U_n \exp[i(\alpha_n^{2\omega} x_1 + \beta_n^{2\omega} x_3)]\hat{x}_2. \tag{11}$$

Thus, we see that the nonlinear efficiencies can be easily calculated from Eq. (9) and the amplitudes U_n of the second-harmonic diffraction orders.

3. EXPERIMENTAL TECHNIQUES

The sinusoidal gratings were made using holographic fabrication techniques. To prepare each surface, a 50 × 50 mm glass plate was coated with a 1.5 μm layer of Shipley S1400-27 photoresist. Each plate was given two exposures, the first being a metered exposure of uniform light from an ultraviolet lamp. This exposure served as a bias so that the total exposure would lie in the linear response region of the photoresist. Then, the plate was exposed to a high-contrast sinusoidal intensity distribution arising at the intersection of two light beams. The source was a HeCd laser of wavelength 442 nm. The plate was developed in a manner known to produce a linear relation between exposure and resulting surface height (30 s in Shipley 352 developer).

The resulting surface was a shallow sinusoidal dielectric grating, whose grating depth was determined from the relative power of its first diffracted order as described elsewhere [57]. This approach employs lowest-order perturbation theory, which appears as an appropriate and accurate method under the experimental conditions (small grating depth, weak first diffracted order). Then, an optically thick layer (400 nm) of silver was evaporated onto the sample at a rate of approximately 1 nm s^{-1} and at a chamber pressure well under 10^{-6} Torr. Thereafter, while not in use, the gratings were kept in an inert gas atmosphere. Consequently, no surface deterioration, sulfidation, or change in optical response was notable during the course of the experiments.

In the experiments studying second-harmonic generation, pulses from a mode-locked Coherent Antares Nd:YAG laser were sent to a Spectra Physics 3800RA injection-seeded regenerative amplifier. The output pulses obtained were of wavelength 1064 nm, full width at half-maximum 100 ps, pulse energy 1 mJ, peak power 10 MW, and repetition rate 1 kHz. The slightly convergent incident beam had transverse width $w = 2.0$ mm at the sample. The sample was mounted on a motorized rotation stage to set the angle of incidence. To measure the second-harmonic diffracted order powers, a detector arm was mounted on a concentric motorized rotation stage that was positioned at the desired diffraction angle. On this arm, 60 cm from the sample, the diffracted light passed through a $CuSO_4$ water-solution cell, a limiting diaphragm, an infrared-absorbing Schott BG39 filter, and a 532 nm interference filter. The diaphragm was large enough to collect all power contained in the diffracted order being detected. Finally, the transmitted

light was focused by a field lens onto a photon-counting photomultiplier.

A Stanford Research SR400 counter was gated to accept photoelectric counts only within a 5 ns window coincident with each laser pulse; the dark counts were thus insignificant. The dead time was 5 ns, which implies that more than one photodetection per laser pulse would be treated as a single count. Rates were thus kept low to avoid detector saturation. The count rate was verified to be linearly proportional to detected second-harmonic power for rates up to 150 s^{-1} and, when signals approached this level, the isolated second-harmonic light was attenuated with calibrated filters placed just before the detector. In all figures, count rates that appear to exceed 150 s^{-1} were actually taken at lower rates with such an attenuation filter and have been corrected for this filter in the data shown. Firing full laser power directly into the detector produced a signal of less than 1 s^{-1}. No metal surface damage or surface plasma was observed during the experiments, which is a consequence of the low 1 mJ pulse energy. As a precaution, the laser power was reduced by approximately one order of magnitude for the few data points taken within one degree of the resonant absorption anomaly at the fundamental frequency; the data were later scaled by the appropriate factor to maintain calibration. In a final step, all data were normalized through comparison with additional measurements of Maker fringes [58] in second-harmonic generation from a window of crystalline quartz for which the nonlinear constants are well established.

4. NUMERICAL AND EXPERIMENTAL RESULTS

In this section, we present experimental data obtained for sinusoidal silver gratings whose fabrication was discussed in Section 3 and compare them with theoretical results obtained by the method described in Section 2. The two gratings studied (gratings A and B) were characterized by their periods d and total groove depth h. For grating A, the parameters are $d = 1.4769$ μm and $h = 46.4$ nm while, for grating B, we find $d = 0.8471$ μm and $h = 29.8$ nm. In calculations, it is necessary to assume values for $\varepsilon_{II}(\omega)$ and $\varepsilon_{II}(2\omega)$; we employ the values estimated in Ref. [23] as $\varepsilon_{II}(\omega) = -67.03 + 2.44i$ and $\varepsilon_{II}(2\omega) = -9.926 + 0.537i$.

As for the nonlinear susceptibilities of the metal, these were measured in Ref. [23] using flat substrates that were silver coated at the same time as gratings A and B. There, the procedure for determining the nonlinear constants consisted of fitting theoretical calculations to the measured second-harmonic reflectivity for different polarization conditions [23]. As discussed earlier, to solve the nonlinear diffraction problem, it is not necessary to know all the bulk and surface susceptibilities individually but only certain combinations of them. In our calculations, as in the free electron model, we assume that $\alpha = 0$. Then, Eq. (4) becomes

$$\chi_{\parallel\parallel\perp} = \chi^s_{ttz}, \tag{12a}$$

$$\chi_{\perp\perp\perp} = \chi^s_{zzz} + \frac{\gamma}{\varepsilon_{II}(2\omega)\varepsilon^2_{II}(\omega)}, \tag{12b}$$

$$\chi_{\perp\parallel\parallel} = \eta_{\perp\parallel\parallel} = \chi^s_{ztt} + \frac{\gamma}{\varepsilon_{II}(2\omega)}, \tag{12c}$$

$$\chi_b = 0. \tag{12d}$$

The particular conventions for the χs vary in the literature. In this paper, we have not counted redundant terms in the calculations of the nonlinear polarizations [59]. In order to find the relationships between the susceptibilities defined in Eqs. (12a)–(12c) and those of Ref. [23], we first obtain the theoretical expression for the second-harmonic efficiency of a flat interface (see Appendix B). Then, by comparing Eqs. (B4) and (B5) with Eqs. (1), (3), and (16) of Ref. [23], we find that

$$\chi_{\parallel\parallel\perp} = \chi'_{\parallel\parallel\perp}, \chi_{\perp\perp\perp} = \frac{\chi'_{\perp\perp\perp}}{2}, \chi_{\perp\parallel\parallel} = \frac{\chi'_{\perp\parallel\parallel}}{2}, \tag{13}$$

where primes denote the susceptibilities measured in Ref. [23]. Then, for our calculation $\chi_{\parallel\parallel\perp} = -6.00 \times 10^{-15}$ cm^2/statvolt, $\chi_{\perp\perp\perp} = 1.52 \times 10^{-17}$ cm^2/statvolt, and $\chi_{\perp\parallel\parallel} = 6.10 \times 10^{-15}$ cm^2/statvolt.

Before presenting the results, it is worth describing qualitatively the physical situations studied. When grating A is illuminated at normal incidence, there are ±1st diffracted orders at ω that appear at ±46° diffraction angle. The 2ω light contains four diffracted orders (±1 and ±2) that appear at ±21° and ±46° at normal incidence. As the angle of incidence is changed, the orders move toward grazing and, for $\theta = 17°$ and p polarization, the +1 order at ω couples to surface plasmon polaritons. The coupling condition for the +1 order at 2ω occurs for $\theta = 44°$ and, for the +2 order at 2ω, at $\theta = 19°$.

With grating B at normal incidence, there are no propagating nonzero diffracted orders at ω while, at 2ω, there are ±1 orders that appear at ±39° diffraction angle. For p polarization, the −1 order at ω couples to surface plasmon polaritons when $\theta = 14°$; the surface plasmon polariton excitation condition at 2ω for p polarization and the +1 order occurs for $\theta = 25°$.

In the figures that follow, we show comparisons between the theoretical curves and the experimental data. For all numerical calculations, we have retained 17 terms in the series expansions, which ensures the convergence of the results to four significant digits. For grating A under s-polarized illumination, theoretical results and experimental data for the zero-order $R_0(2\omega)$ are shown in Figs. 2(a) and 2(b). It is seen that the overall agreement between the theoretical and experimental results is quite good. The main feature present is an s-shaped or Fano-like feature in both the calculations and the experimental data at 44°, which is the angle that the +1 order at 2ω couples to plasmon polaritons. For grating B, analogous results for $R_0(2\omega)$ are shown in Figs. 2(c) and 2(d), which present even better theoretical/experimental agreement. Here, a similar feature appears at 25°, which again coincides with plasmon polariton excitation in the +1 order at 2ω.

In Fig. 2, the quantitative agreement between the theoretical and experimental results is, by itself, a significant result that is worth pointing out. We recall that there are no fitting parameters in the theory and that the experimental data were normalized in a manner consistent with the theory. It is also notable that, even with rates under 100 detected photons s^{-1} throughout Fig. 2, the experimental curves are clear and do not have excessive noise or background. Indeed, Fig. 2 presents the lowest overall signal levels of all data to be shown here. We also add that, when

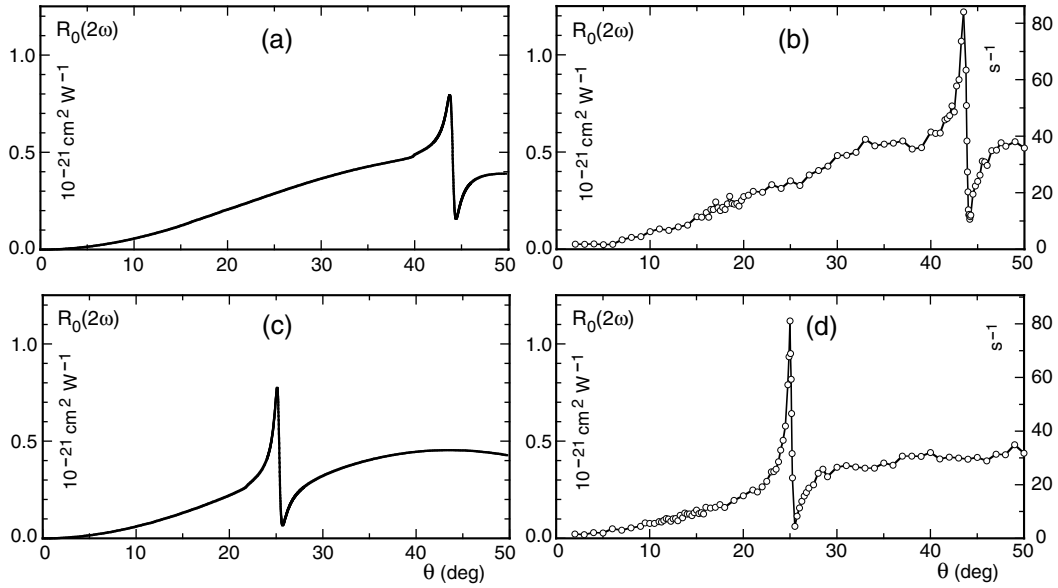

Fig. 2. For *s* incident polarization, second-harmonic grating efficiency $R_0(2\omega)$ as a function of incidence angle θ. Shown are theoretical results for grating A in (a), to be compared with the normalized experimental data in (b). For grating B, theoretical results in (c) are to be compared with the experimental data in (d). The vertical axes at the far right show photocount rates, and the light detected was confirmed to be *p*-polarized.

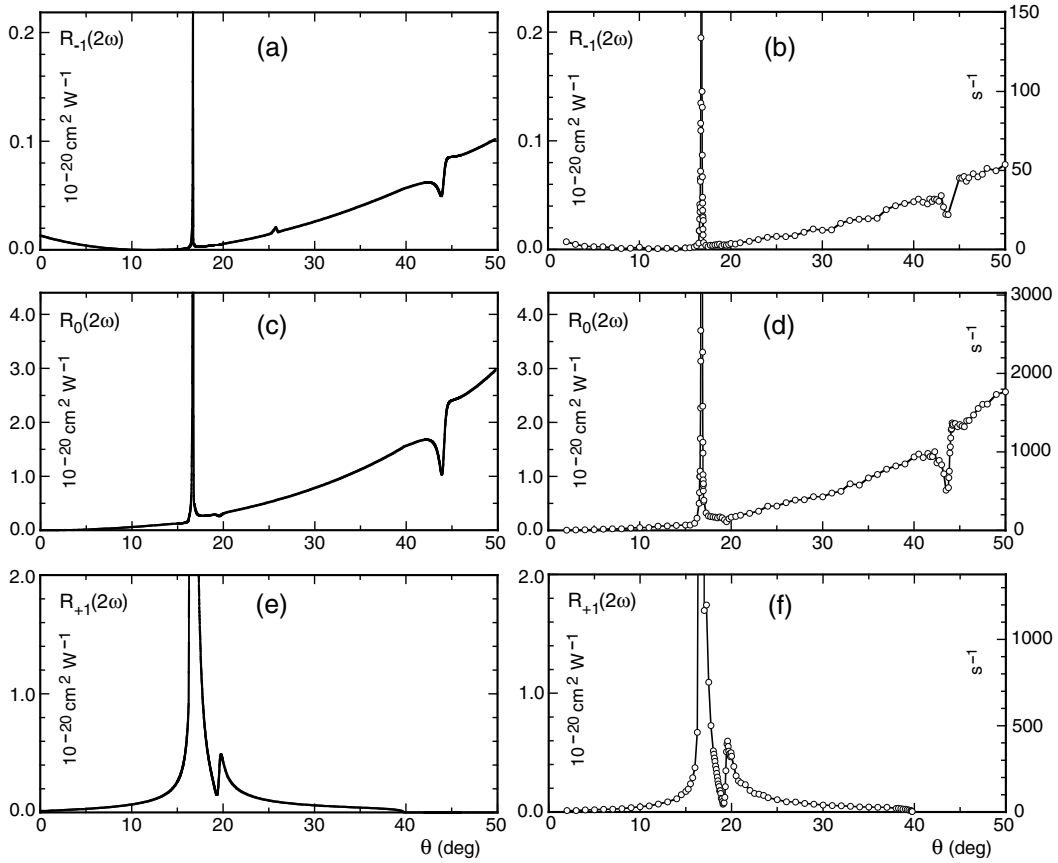

Fig. 3. For grating A in *p* incident polarization, second-harmonic efficiency $R_n(2\omega)$ for orders $n = -1$, 0, and $+1$ as indicated. (a, c, e) Theoretical results are to be compared with (b, d, f) corresponding experimental data, respectively. The vertical axes at the far right show photocount rates. At an incidence angle of $\theta \approx 17°$, the results rise off-scale to (a) 0.29×10^{-20}, (b) 0.75×10^{-20}, (c) 4.7×10^{-19}, (d) 4.6×10^{-19}, (e) 2.7×10^{-17}, and (f) 1.8×10^{-17}.

illuminating the surface with a laser at 2ω, deep resonant absorption anomalies appear in the zero orders of both gratings A and B. These have the usual form of a simple dip and appear at the same angles as the Fano-like features of Fig. 2. We do not present these linear-optics results here but simply emphasize that the features seen in Fig. 2 are quite different from the linear case. Another notable difference is that the anomalies in linear optics require p incident polarization, while the features of Fig. 2 are seen for s incident polarization (even though, of course, the s incident field at ω produces the diffracted order at 2ω in pure p polarization).

We now move on to results obtained with p-polarized illumination. In Fig. 3, we show such theoretical and experimental results for $R_n(2\omega)$ for grating A as a function θ for $n = -1$, 0, and $+1$. Generally, the results for $R_{-1}(2\omega)$ [Figs. 3(a) and 3(b)] resemble those for $R_0(2\omega)$ [Figs. 3(c) and 3(d)], although the latter are approximately 1.5 orders of magnitude higher. In the case of $R_{+1}(2\omega)$, the curves take on a somewhat different shape, and fall to zero as this order reaches grazing at $\theta = 40°$.

All curves throughout Fig. 3 present their highest levels in the narrow peaks at $\theta = 17°$, which rise above the full scale of the plots. As mentioned earlier, this angle corresponds to the strong plasmon polariton excitation arising through the $+1$st diffracted order at ω; thus, this condition fully dominates the curves for $R_n(2\omega)$. However, there are other features seen in the results; for example, the feature at $\theta = 44°$ in Figs. 3(a)–3(d) coincides with the $+1$-order excitation at 2ω of a plasmon polariton as had been noted earlier in Figs. 2(a) and 2(b), although the features seen in Figs. 3(a)–3(d) take on a somewhat different shape. It is perhaps of interest that this 2ω plasmon polariton excitation arises from the $+1$ order plotted in Figs. 2(e) and 2(f), which reaches grazing at 40° and, for slightly larger θ, produces the excitation seen indirectly in the other orders.

Other features seen in Fig. 3 include subtle minimums at 19° in both theoretical and experimental results for $R_0(2\omega)$ [Figs. 3(c) and 3(d)] and $R_{+1}(2\omega)$ [Figs. 3(e) and 3(f)]; as noted earlier, this angle is associated with plasmon polariton coupling in the $+2$ order at 2ω. The feature produced is quite subtle in $R_0(2\omega)$, but it is much deeper in $R_{+1}(2\omega)$, where it falls slightly to the left of that in $R_0(2\omega)$ in both the theoretical and experimental results. Finally, there is a small peak at 26° in the theoretical result for $R_{-1}(2\omega)$ [Fig. 3(a)], which is the angle at which the grating couples to an ω plasmon polariton in the -2 order. This peak is not apparent in the corresponding experimental result [Fig. 3(b)], but its height may be comparable to the experimental noise levels.

It must be stressed that, throughout Fig. 3, the general agreement between theoretical and experimental results is remarkably good. Once again, this is true both in the absolute vertical scale of results as well as in the shape of the features seen in the curves. Still, there are some differences, for example, in the height of the strong peaks at 17°, which we have found

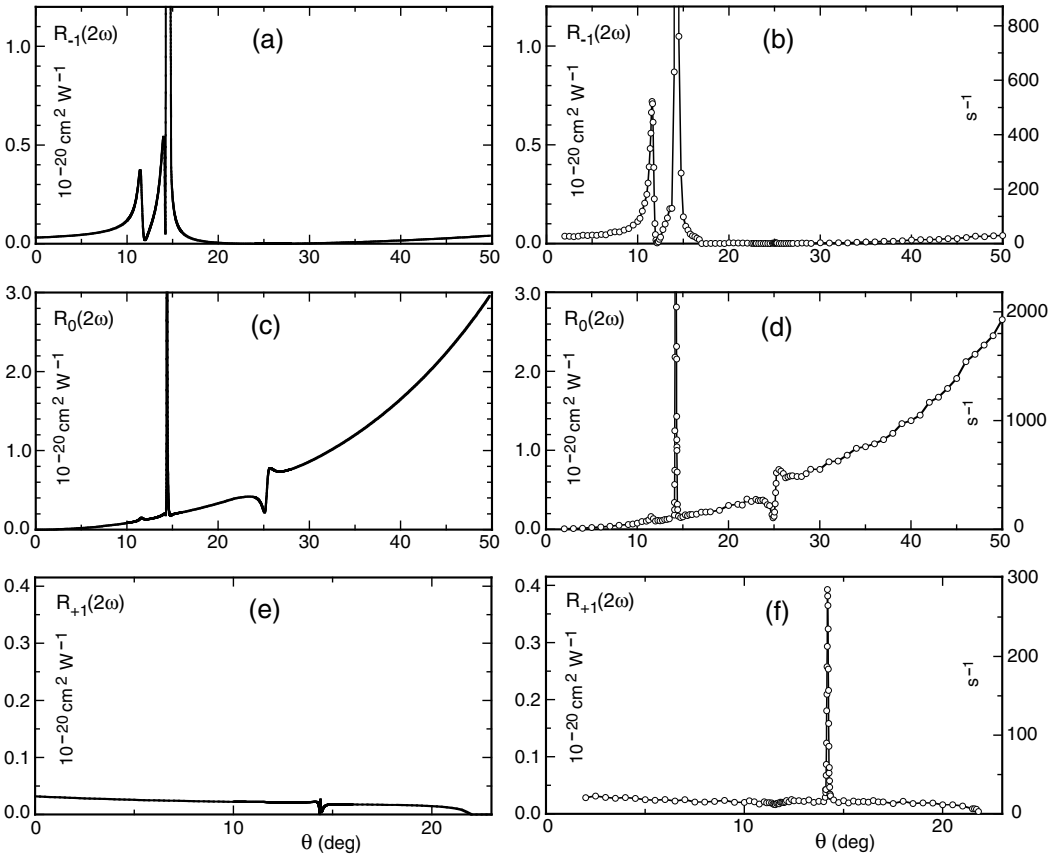

Fig. 4. For grating B in p incident polarization, second-harmonic efficiency $R_n(2\omega)$ for orders $n = -1$, 0, and $+1$ as indicated. (a),(c), (e) Theoretical results are to be compared with (b),(d),(f) corresponding experimental data, respectively. The vertical axes at the far right show photocount rates. At incidence angle $\theta \approx 14°$, the results rise off-scale to (a) 2.5×10^{-17}, (b) 1.9×10^{-17}, (c) 2.5×10^{-19}, and (d) 2.6×10^{-19}.

computationally to be quite sensitive to small changes in the metal's constants and in the surface profile function. Further, there are modest scale differences seen upon close examination of Fig. 3. Nevertheless, in many respects, the general level of theoretical and experimental agreement throughout Fig. 3 is quite notable.

We now consider Fig. 4, which shows, for the other grating (grating B) in p polarization, theoretical and experimental results for $R_n(2\omega)$ with $n = -1$, 0, and $+1$. For grating B, the strong plasmon polariton coupling at ω occurs in the -1 order at $\theta = 14°$, and corresponding high off-scale peaks are seen there in Fig. 4. The heights of these peaks are more consistent in the theoretical/experimental comparisons in Figs. 4(a) and 4(b) and 4(c) and 4(d) than had been the case in Fig. 3. An obvious disagreement is the theoretical result for $R_{+1}(2\omega)$ [Fig. 4(e)] which, unlike the experiment, shows a feature with no peak at all at 14°. We have found that, by changing the metal dielectric constants, or by adding a weak second harmonic to the *surface profile*, a peak in Fig. 4(e) can be made to rise up to the experimental levels. However, we consider this to be a minor issue since these peaks in other cases of Fig. 4 can be well over three orders of magnitude higher and already present good theoretical/experimental comparisons.

The other features apparent in Fig. 4 include that seen at 25° in $R_0(2\omega)$, which arises from plasmon polariton excitation in the $+1$ order at 2ω; as in Fig. 3, this arises for θ slightly greater than that for which the $+1$ order reaches grazing [22°, see Figs. 4(e) and 4(f)]. There is also a low peak at 12° in $R_0(2\omega)$ coinciding with plasmon polariton excitation in the -2 order at 2ω; this peak nearly aligns with far more distinct peaks in $R_{-1}(2\omega)$. Throughout all of these features, the theoretical/experimental comparison is reasonable, with some differences in scale in some cases but outstanding comparisons in others.

To summarize the results that have been presented here, for p incident polarization as in Figs. 3 and 4, all orders at 2ω are purely p-polarized and reach their highest levels when a ± 1 diffracted order at ω produces plasmon polariton excitation. For positive θ, if the $+1$ order at ω produces the coupling, the highest levels of all appear in $R_{+1}(2\omega)$, while if it is the -1 order at ω, they are found in $R_{-1}(2\omega)$. In addition, other distinct features are seen in $R_n(2\omega)$ that are related to plasmon polariton excitation at either ω or 2ω. On the other hand, in the case of s incident polarization as in Fig. 2, there is never any plasmon polariton excitation at ω. Consequently, the cases studied for $R_0(2\omega)$ are at quite low levels, are purely p-polarized, and only contain features arising from plasmon polariton excitation at 2ω. The theoretical and experimental results are not only in qualitative agreement on all of these points but, in many cases, the results are remarkably close in terms of quantitative agreement.

5. SUMMARY AND CONCLUSIONS

We have presented a quantitative comparison between experimental and theoretical results of the second-harmonic efficiency generated by sinusoidal silver diffraction gratings. Experiments with characterized sinusoidal silver gratings were carried out, in which the second-harmonic power was properly normalized through comparison with a quartz reference sample. These experiments have produced reliable data down to levels corresponding to only a few tens of detected photons per second, with negligible background. The nonlinear grating order efficiency was accurately measured at unprecedented low levels, without the surface damage common in other experimental approaches.

Starting from a general expression for the nonlinear polarization, we have developed a Rayleigh method to calculate the surface-generated second-harmonic signal in terms of the nonlinear susceptibilities. The Rayleigh method is well-suited to the shallow gratings studied, and the treatment of the nonlinearities is fairly general and does not introduce restrictive approximations. Employing previously measured values of the nonlinear susceptibilities of a flat silver surface, we have obtained good agreement between the experimental and theoretical results over a wide range of levels, not only in the shape of the nonlinear efficiencies but also in their absolute values. The degree of agreement is quite notable and demonstrates that the experimentally determined nonlinear constants for flat surfaces can be used to study plasmonic effects quantitatively with rigorous calculations.

APPENDIX A: ELEMENTS OF THE MATRIX EQUATION

In what follows, we assume that medium I is vacuum [$\varepsilon_I(\omega) = \varepsilon_I(2\omega) = 1$]. The matrix elements are given by

$$A^{>}_{mn} = \int_0^1 \exp[i(\alpha_n^{2\omega} - \alpha_m^{2\omega})f(t)]\exp(i\beta_n^{2\omega}g(t))\mathrm{d}t, \quad \textbf{(A1)}$$

$$A^{<}_{mn} = -\int_0^1 \exp[i(\alpha_n^{2\omega} - \alpha_m^{2\omega})f(t)]\exp(i\gamma_n^{2\omega}g(t))\mathrm{d}t, \quad \textbf{(A2)}$$

$$B^{>}_{mn} = \int_0^1 h_n^{>}(t)\exp[i(\alpha_n^{2\omega} - \alpha_m^{2\omega})f(t)]\exp(i\beta_n^{2\omega}g(t))\mathrm{d}t, \quad \textbf{(A3)}$$

$$B^{<}_{mn} = -\frac{1}{\varepsilon_{II}(2\omega)}\int_0^1 h_n^{<}(t)\exp[i(\alpha_n^{2\omega} - \alpha_m^{2\omega})f(t)] \times \exp(i\gamma_n^{2\omega}g(t))\mathrm{d}t, \quad \textbf{(A4)}$$

where

$$h_n^{>}(t) = i[-g'(t)\alpha_n^{2\omega} + \beta_n^{2\omega}f'(t)], \quad \textbf{(A5)}$$

$$h_n^{<}(t) = i[-g'(t)\alpha_n^{2\omega} + \gamma_n^{2\omega}f'(t)]. \quad \textbf{(A6)}$$

The nonlinear sources can be written as follows:

$$u^s_m = 0, \quad \textbf{(A7)}$$

$$v^s_m = \frac{16\pi i\omega}{c}\eta_{\perp\|\|}\left\{i\psi_{0s}^2\int_0^1 \mathcal{C}E_1(m|t)\mathrm{d}t + i\psi_{0s}\sum_n R^s_n\int_0^1(\mathcal{C}+\mathcal{F}_n)E_2(n,m|t)\mathrm{d}t + i\sum_{n,l}R^s_nR^s_l\int_0^1\mathcal{F}_lE_3(n,m,l|t)\mathrm{d}t\right\}, \quad \textbf{(A8)}$$

$$u_m^p = \frac{8\pi i c}{\omega}\chi_{\parallel\parallel\perp}\left\{-\psi_{0p}^2\int_0^1 \frac{1}{\phi^2}\mathcal{B}\mathcal{C}E_1(m|t)\mathrm{d}t + \psi_{0p}\sum_n R_n^p\int_0^1\frac{1}{\phi^2}(\mathcal{E}_n\mathcal{C}-\mathcal{F}_n\mathcal{B})E_2(n,m|t)\mathrm{d}t + \sum_{n,l}R_n^pR_l^p\int_0^1\frac{1}{\phi^2}\mathcal{E}_n\mathcal{F}_lE_3(n,m,l|t)\mathrm{d}t\right\}, \tag{A9}$$

$$v_m^p = \frac{-16\pi i c}{\omega}\left\{\psi_{0p}^2\int_0^1\left[\chi_{\perp\perp\perp}\left(\frac{\phi'}{\phi^3}\mathcal{C}^2-\frac{1}{\phi^2}\mathcal{C}\mathcal{G}\right) + \chi_{\perp\parallel\parallel}\left(\frac{\phi'}{\phi^3}\mathcal{B}^2-\frac{1}{\phi^2}\mathcal{B}\mathcal{H}\right)+i\chi_b\mathcal{C}\right]E_1(m|t)\mathrm{d}t + \psi_{0p}\sum_n R_n^p\int_0^1\left[\chi_{\perp\perp\perp}\left(\frac{\phi'}{\phi^3}2\mathcal{C}\mathcal{F}_n-\frac{1}{\phi^2}(\mathcal{C}\mathcal{J}_n+\mathcal{G}\mathcal{F}_n)\right) - \chi_{\perp\parallel\parallel}\left(\frac{\phi'}{\phi^3}2\mathcal{B}\mathcal{E}_n-\frac{1}{\phi^2}(\mathcal{B}\mathcal{I}_n+\mathcal{H}\mathcal{E}_n)\right)+i\chi_b(\mathcal{F}_n+\mathcal{C})\right] \times E_2(n,m|t)\mathrm{d}t + \sum_{n,l}R_n^pR_l^p\int_0^1\left[\chi_{\perp\perp\perp}\left(\frac{\phi'}{\phi^3}\mathcal{F}_n\mathcal{F}_l-\frac{1}{\phi^2}\mathcal{F}_n\mathcal{J}_l\right) + \chi_{\perp\parallel\parallel}\left(\frac{\phi'}{\phi^3}\mathcal{E}_n\mathcal{E}_l-\frac{1}{\phi^2}\mathcal{E}_n\mathcal{I}_l\right)+i\chi_b\mathcal{F}_l\right] \times E_3(n,m,l|t)\mathrm{d}t\right\}, \tag{A10}$$

where $\phi=\phi(t)$, $\phi'=d\phi(t)/dt$, $\psi_{0\kappa}$ is the amplitude of the incident field for s or p polarization, R_n^κ is the Rayleigh amplitude of the nth reflected order at ω for s or p polarization, and

$$E_1(m|t)=\exp\{-i[(2\pi/d)mf(t)+2\beta_0^\omega g(t)]\}, \tag{A11}$$

$$E_2(n,m|t)=\exp\{i[(2\pi/d)(n-m)f(t)+(\beta_n^\omega-\beta_0^\omega)g(t)]\}, \tag{A12}$$

$$E_3(n,m,l|t)=\exp\{i[(2\pi/d)(n+l-m)f(t)+(\beta_n^\omega+\beta_l^\omega)g(t)]\}. \tag{A13}$$

Also, the functions denoted by calligraphic letters are functions of the parameter t and are given by

$$\mathcal{B}=\alpha_0^\omega g'(t)+\beta_0^\omega f'(t),\quad \mathcal{C}=\alpha_0^\omega f'(t)-\beta_0^\omega g'(t),$$
$$\mathcal{G}=(\mathcal{C})'+i(\mathcal{C})^2,\quad \mathcal{H}=(\mathcal{B})'+i\mathcal{B}\mathcal{C},$$
$$\mathcal{E}_j=-\alpha_j^\omega g'(t)+\beta_j^\omega f'(t),\quad \mathcal{F}_j(t)=\alpha_j^\omega f'(t)+\beta_j^\omega g'(t),$$
$$\mathcal{I}_j=(\mathcal{E}_j)'+i\mathcal{E}_j\mathcal{F}_j,\quad \mathcal{J}_j=(\mathcal{F}_j)'+i(\mathcal{F}_j)^2.$$

In these expressions, the primes denote differentiation with respect to the parameter t, and α_j^ω and β_j^ω are defined as in Eqs. (6a) and (6c) but for the frequency ω.

APPENDIX B: EFFICIENCY FOR A FLAT INTERFACE

Let us consider the reflected second-harmonic efficiency for a flat interface. In this case, only the specular order propagates ($n=0$). Therefore Eq. (9) can be written as

$$R_0(2\omega)=\frac{S_0^{2\omega}}{(S_i)^2}. \tag{B1}$$

The modulus of the time-averaged Poynting vector for the zeroth order is given by

$$S_0^{2\omega}=\frac{c}{8\pi}|U_0|^2, \tag{B2}$$

where U_0 is the complex amplitude of the unique term ($n=0$) that remains from Eq. (5a). By using the nonlinear boundary conditions in Eq. (2), we obtain

$$U_0=\frac{[-\gamma_0^{2\omega}A_p(\omega)/\varepsilon_{\mathrm{II}}(2\omega)+iB_p(\omega)]\exp(-i\alpha_0^{2\omega}x_1)}{\beta_0^{2\omega}+\gamma_0^{2\omega}/\varepsilon_{\mathrm{II}}(2\omega)}. \tag{B3}$$

We note that for flat interfaces, the nonlinear sources $A_p(\omega)$ and $B_p(\omega)$ [see Eq. (3)] can be written in analytical form. After some algebra, we find that the second-harmonic efficiency is given by

$$R_0(2\omega)=\frac{32\pi^3\omega^2}{c^3}\mathrm{tg}^2\theta\left|t_p^2(\omega)t_p(2\omega)n_{\mathrm{II}}(2\omega)\left\{\frac{\sin^2\theta}{\varepsilon_{\mathrm{II}}(\omega)}\times(\varepsilon_{\mathrm{II}}^2(\omega)2\chi_{\perp\perp\perp}-2\chi_{\perp\parallel\parallel})+2\chi_{\perp\parallel\parallel} -2\frac{\sqrt{\varepsilon_{\mathrm{II}}(\omega)-\sin^2\theta}\sqrt{\varepsilon_{\mathrm{II}}(2\omega)-\sin^2\theta}}{\varepsilon_{\mathrm{II}}(2\omega)}\chi_{\parallel\parallel\perp}\right\}\right|^2, \tag{B4}$$

for p-polarized illumination, and

$$R_0(2\omega)=\frac{32\pi^3\omega^2}{c^3}\mathrm{tg}^2\theta|t_s^2(\omega)t_p(2\omega)n_{\mathrm{II}}(2\omega)2\chi_{\perp\parallel\parallel}|^2, \tag{B5}$$

for s-polarized illumination. The Fresnel transmission coefficients $t_p(\Omega)$ and $t_s(\omega)$ that appear in Eqs. (B4) and (B5) are given by the following expressions:

$$t_p(\Omega)=\frac{2n_{\mathrm{II}}(\Omega)\cos\theta}{\varepsilon_{\mathrm{II}}(\Omega)\cos\theta+\sqrt{\varepsilon_{\mathrm{II}}(\Omega)-\sin^2\theta}}, \tag{B6}$$

$$t_s(\omega)=\frac{2\cos\theta}{\cos\theta+\sqrt{\varepsilon_{\mathrm{II}}(\omega)-\sin^2\theta}}, \tag{B7}$$

where Ω stands for the fundamental (ω) or second-harmonic (2ω) frequencies. By comparing Eqs. (B4) and (B5) with Eqs. (1), (3), and (16) of Ref. [23], we find the relationships given in Eq. (13).

Funding. Consejo Nacional de Investigaciones Científicas y Técnicas (CONICET) (PIP 112-200801-01880, PIP 451); Universidad de Buenos Aires (UBA) (UBACyT 20020100100533, UBACyT 20020150100028BA); Universidad Autónoma de Baja California (UABC); Consejo Nacional de Ciencia y Tecnología (CONACYT) (181669, 253640, FON.INST./23/2016 No. 189).

Acknowledgment. M. Inchaussandague and M. Gigli gratefully acknowledge support from CONICET and UBA. C. Valencia gratefully acknowledges support from UABC (Programa de Movilidad Académica). The work of E. Méndez and K. O'Donnell has been partially supported by the CONACYT.

REFERENCES

1. J. C. Maxwell Garnett, "Colours in metal glasses and in metallic films," Philos. Trans. R. Soc. London A **203**, 385–420 (1904).
2. H. Raether, *Surface Plasmons on Smooth and Rough Surfaces and Gratings* (Springer-Verlag, 1988).
3. A. V. Zayats, I. I. Smolyaninov, and A. A. Maradudin, "Nano-optics of surface plasmon polaritons," Phys. Rep. **408**, 131–314 (2005).
4. W. L. Barnes, "Surface plasmon-polariton length scales: a route to sub-wavelength optics," J. Opt. A **8**, S87–S93 (2006).
5. J. M. Pitarke, V. M. Silkin, E. V. Chulkov, and P. M. Echenique, "Theory of surface plasmons and surface-plasmon polaritons," Rep. Prog. Phys. **70**, 1–87 (2007).
6. S. A. Maier, *Plasmonics: Fundamentals and Applications* (Springer, 2007).
7. F. Brown, R. E. Parks, and A. M. Sleeper, "Nonlinear optical reflection from a metallic boundary," Phys. Rev. Lett. **14**, 1029–1031 (1965).
8. F. Brown and R. E. Parks, "Magnetic-dipole contribution to optical harmonics in silver," Phys. Rev. Lett. **16**, 507–509 (1966).
9. N. Bloembergen, R. K. Chang, and C. H. Lee, "Second harmonic generation of light in reflection from media with inversion symmetry," Phys. Rev. Lett. **16**, 986–989 (1966).
10. N. Bloembergen, R. K. Chang, S. S. Jha, and C. H. Lee, "Optical second-harmonic generation in reflection from media with inversion symmetry," Phys. Rev. B **174**, 813–822 (1968).
11. C. S. Wang and A. N. Duminski, "Second-harmonic generation of light at the boundary of alkali halides and glasses," Phys. Rev. Lett. **20**, 668–671 (1968).
12. J. Rudnick and E. A. Stern, "Second-harmonic radiation from metal surfaces," Phys. Rev. B **4**, 4274–4290 (1971).
13. J. E. Sipe, C. Y. So, V. Fukui, and G. I. Stegeman, "Analysis of second-harmonic generation at metal surfaces," Phys. Rev. B **21**, 4389–4402 (1980).
14. J. E. Sipe and G. I. Stegeman, "Nonlinear optical response of metal surfaces," in *Surface Polaritons*, V. M. Agranovich and D. L. Mills, eds. (North-Holland, 1982).
15. T. F. Heinz, "Nonlinear optics of surfaces and adsorbates," Ph.D. thesis (University of California, 1982).
16. M. Corvi and W. L. Schaich, "Hydrodynamic-model calculation of second-harmonic generation at a metal surface," Phys. Rev. B **33**, 3688–3695 (1986).
17. A. Liebsch, "Second-harmonic generation at simple metal surfaces," Phys. Rev. Lett. **61**, 1233–1236 (1988).
18. J. A. Maytorena, W. L. Mochán, and B. S. Mendoza, "Hydrodynamic model for second-harmonic generation at conductor surfaces with continuous profiles," Phys. Rev. B **51**, 2556–2562 (1995).
19. B. S. Mendoza and W. L. Mochán, "Exactly solvable model of surface second-harmonic generation," Phys. Rev. B **53**, 4999–5006 (1996).
20. J. L. Coutaz, D. Maystre, M. Nevière, and R. Reinisch, "Optical second-harmonic generation from silver at 1.064 μm pump wavelength," J. Appl. Phys. **62**, 1529–1531 (1987).
21. N. V. Akhmediev, I. V. Melnikov, and L. J. Robur, "Second-harmonic generation by a reflecting metal surface," Laser Phys. **4**, 1194–1197 (1994).
22. D. Krause, C. W. Teplin, and C. T. Rogers, "Optical surface second harmonic measurements of isotropic thin-film metals: gold, silver, copper, aluminum and tantalum," Phys. Rev. B **6**, 3626–3634 (2004).
23. K. A. O'Donnell and R. Torre, "Characterization of the second-harmonic response of a silver–air interface," New J. Phys. **7**, 154 (2005).
24. A. Wokaun, J. G. Bergman, J. P. Heritage, A. M. Glass, P. F. Liao, and D. H. Olson, "Surface second-harmonic generation from metal island films and microlithographic structures," Phys. Rev. B **24**, 849–856 (1981).
25. R. Reinisch and M. Nevière, "Electromagnetic theory of diffraction in nonlinear optics and surface-enhanced nonlinear optical effects," Phys. Rev. B **28**, 1870–1885 (1983).
26. G. A. Farias and A. A. Maradudin, "Second harmonic generation in reflection from a metallic grating," Phys. Rev. B **30**, 3002–3015 (1984).
27. J. L. Coutaz, M. Nevière, E. Pic, and R. Reinisch, "Experimental study of surface-enhanced second-harmonic generation on silver gratings," Phys. Rev. B **32**, 2227–2232 (1985).
28. E. Popov and M. Nevière, "Surface-enhanced second-harmonic generation in nonlinear corrugated dielectrics: new theoretical approaches," J. Opt. Soc. Am. B **11**, 1555–1564 (1994).
29. A. C. R. Pipino, R. P. Van Duyne, and G. C. Schatz, "Surface-enhanced second-harmonic diffraction: experimental investigation of selective enhancement," Phys. Rev. B **53**, 4162–4169 (1996).
30. D. B. Singh and V. K. Tripathi, "Surface plasmon excitation at second harmonic over a rippled surface," J. Appl. Phys. **102**, 083301 (2007).
31. M. D. McMahon, R. Lopez, R. F. Haglund, Jr., E. A. Ray, and P. H. Bunton, "Second-harmonic generation from arrays of symmetric gold nanoparticles," Phys. Rev. B **73**, 041401 (2006).
32. T. Xu, X. Jiao, G. P. Zhang, and S. Blair, "Second-harmonic emission from subwavelength apertures: effects of aperture symmetry and lattice arrangement," Opt. Express **15**, 13894–13906 (2007).
33. A. Lesuffleur, L. K. Swaroop Kumar, and R. Gordon, "Enhanced second harmonic generation from nanoscale double-hole arrays in a gold film," Appl. Phys. Lett. **88**, 261104 (2006).
34. M. Kauranen and A. V. Zayats, "Nonlinear plasmonics," Nat. Photonics **6**, 737–748 (2012).
35. J. Butet, P.-F. Brevet, and O. J. F. Martin, "Optical second harmonic generation in plasmonic nanostructures: from fundamental principles to advanced applications," ACS Nano **9**, 10545–10562 (2015).
36. R. T. Deck and R. K. Grygier, "Surface-plasmon enhanced harmonic generation at a rough metal surface," Appl. Opt. **23**, 3202–3213 (1984).
37. K. A. O'Donnell, R. Torre, and C. S. West, "Observations of second-harmonic generation from randomly rough metal surfaces," Phys. Rev. B **55**, 7985–7992 (1997).
38. K. A. O'Donnell, R. Torre, and C. S. West, "Observations of backscattering effects in second-harmonic generation from a weakly rough metal surface," Opt. Lett. **21**, 1738–1740 (1996).
39. M. A. Leyva-Lucero, E. R. Méndez, T. A. Leskova, A. A. Maradudin, and J. Q. Lu, "Multiple-scattering effects in the second-harmonic generation of light in reflection from a randomly rough metal surface," Opt. Lett. **21**, 1809–1811 (1996).
40. K. A. O'Donnell and R. Torre, "Second-harmonic generation from a strongly rough metal surface," Opt. Commun. **138**, 341–344 (1997).
41. M. A. Leyva-Lucero, E. R. Méndez, T. A. Leskova, and A. A. Maradudin, "Destructive interference effects in the second harmonic light generated at randomly rough metal surfaces," Opt. Commun. **161**, 79–94 (1999).
42. T. A. Leskova, A. A. Maradudin, and E. R. Méndez, "Multiple-scattering phenomena in the second-harmonic generation of light reflected from and transmitted through randomly rough metal surfaces," in *Optical Properties of Nanostructured Random Media*, V. M. Shalaev, ed. (Springer, 2002).
43. B. Lamprecht, A. Leitner, and F. R. Aussenegg, "Femtosecond decay-time measurement of electron-plasma oscillation in nanolithographically designed silver particles," Appl. Phys. B **64**, 269–272 (1997).
44. H. Tuovinen, M. Kauranen, K. Jefimovs, P. Vahimaa, T. Vallius, J. Turunen, N. V. Tkachenko, and H. Lemmetyinen, "Linear and second-order nonlinear optical properties of arrays of noncentrosymmetric gold nanoparticles," J. Nonlinear Opt. Phys. Mater. **11**, 421–432 (2002).
45. B. K. Canfield, S. Kujala, K. Jefimovs, J. Turunen, and M. Kauranen, "Linear and nonlinear optical responses influenced by broken symmetry in an array of gold nanoparticles," Opt. Express **12**, 5418–5423 (2004).
46. M. W. Klein, C. Enkrich, M. Wegener, and S. Linden, "Second-harmonic generation from magnetic meta-materials," Science **313**, 502–504 (2006).

47. M. W. Klein, M. Wegener, N. Feth, and S. Linden, "Experiments on second- and third-harmonic generation from magnetic metamaterials," Opt. Express **15**, 5238–5247 (2007).
48. N. Feth, S. Linden, M. W. Klein, M. Decker, F. B. P. Niesler, Y. Zeng, W. Hoyer, J. Liu, S. W. Koch, J. V. Moloney, and M. Wegener, "Second-harmonic generation from complementary split-ring resonators," Opt. Lett. **33**, 1975–1977 (2008).
49. Lord Rayleigh, "On the dynamical theory of gratings," Proc. R. Soc. London A **79**, 399–416 (1907).
50. S. O. Rice, "Reflection of electromagnetic waves from slightly rough surfaces," Commun. Pure Appl. Math. **4**, 351–378 (1951).
51. C. I. Valencia, E. R. Méndez, and B. S. Mendoza, "Second-harmonic generation in the scattering of light by two-dimensional particles," J. Opt. Soc. Am. B **20**, 2150–2161 (2003).
52. M. L. Gigli, M. E. Inchaussandague, C. I. Valencia, and E. R. Méndez, "Nonlinear electromagnetic response of corrugated metallic gratings," J. Opt. Soc. Am. B **28**, 1940–1950 (2011).
53. J. P. Hugonin, R. Petit, and M. Cadilhac, "Plane-wave expansions used to describe the field diffracted by a grating," J. Opt. Soc. Am. **71**, 593–598 (1981).
54. A. Wirgin, "Plane-wave expansions used to describe the field diffracted by a grating: comments," J. Opt. Soc. Am. **72**, 812–813 (1982).
55. R. A. Depine and M. L. Gigli, "Diffraction from corrugated gratings made with uniaxial crystals: Rayleigh methods," J. Mod. Opt. **41**, 695–715 (1994).
56. R. A. Depine and M. L. Gigli, "Conversion between polarization states at the sinusoidal boundary of a uniaxial crystal," Phys. Rev. B **49**, 8437–8445 (1994).
57. D. Heitmann, "Diffraction of light from weakly modulated silver surfaces," Opt. Commun. **20**, 292–297 (1977).
58. J. Jerphagnon and S. K. Kurtz, "Maker fringes: a detailed comparison of theory and experiment for isotropic and uniaxial crystals," J. Appl. Phys. **41**, 1667–1681 (1970).
59. Y. R. Shen, *The Principles of Nonlinear Optics* (Wiley, 1984).